

# A probabilistic solution to geophysical inverse problems in complex variables and its application to complex resistivity imaging

Joost Hase<sup>1</sup>, Maximilian Weigand<sup>1</sup> and Andreas Kemna<sup>1</sup>

Geophysics Section, Institute of Geosciences, University of Bonn, Bonn 53115, Germany. E-mail: [hase@geo.uni-bonn.de](mailto:hase@geo.uni-bonn.de)

Accepted 2024 January 31. Received 2024 January 25; in original form 2023 December 21

## SUMMARY

We introduce a novel probabilistic framework for the solution of non-linear geophysical inverse problems in complex variables. By using complex probability distributions, this approach can simultaneously account for individual errors of real and imaginary data parts, independently regularize real and imaginary parts of the complex model, and still take into account cross-sensitivities resulting from a complex forward calculation. The inverse problem is solved by means of optimization. An application of the framework to complex resistivity (CR) imaging demonstrates its advantages over the established inversion approach for CR measurements. We show that CR data, with real and imaginary parts being subject to different errors, can be fitted adequately, accounting for the individual errors and applying independent regularization to the real and imaginary part of the subsurface conductivity. The probabilistic framework itself serves as a basis for the future application of global sampling approaches, such as Markov chain Monte Carlo methods.

**Key words:** Inverse theory - Bayesian inference - Induced polarization - Tomography.

## 1 INTRODUCTION

We introduce a probabilistic framework for the solution of geophysical inverse problems in complex variables. Within the framework, data and model parameters are treated explicitly as complex random variables and we use Bayes' theorem to combine the complex probability distributions associated with likelihood and model prior into a posterior model distribution. The probabilistic formulation of the inverse problem using Bayes' theorem inherently accounts for data errors and uncertainties in the prior assumptions, both of which are propagated naturally into the solution (e.g. Bayes 1763; Sen & Stoffa 1996; Tarantola 2005). Sampling strategies, such as Markov chain Monte Carlo (MCMC) methods, can be employed to numerically approximate statistical estimators of interest over the posterior distribution and to explore ambiguities in the solution (e.g. Sambridge & Mosegaard 2002). Applications of this concept to geophysical inverse problems in real variables can be found in many different fields of geophysics (e.g. Sen & Stoffa 1996; De Pasquale *et al.* 2019; Fichtner *et al.* 2019; Deng *et al.* 2022). However, to our knowledge, the concept has not yet been extended to geophysical inverse problems in complex variables. The application of MCMC strategies to the general geoelectric imaging problem is still challenging, mainly due to the computational cost of evaluating the forward response. Because of this, we exclusively focus on the estimation of the maximum a posteriori (MAP) solution by means of Gauss–Newton optimization and leave the adaptation of sampling strategies to the introduced probabilistic framework open to future research. The considerations with regard to complex

differentiability, necessary for the application of Gauss–Newton optimization, provide a basis for the application of gradient-guided MCMC methods, such as Hamiltonian Monte Carlo (e.g. Neal *et al.* 2011; Fichtner *et al.* 2019).

The complex resistivity (CR) method targets the distribution of the complex electrical conductivity within the subsurface, capturing the conduction and polarization properties under the application of an alternating current at a given frequency. In CR surveys, the induced polarization response of the subsurface is measured and analysed in terms of the frequency-dependent complex electrical impedance (e.g. Van Voorhis *et al.* 1973; Pelton *et al.* 1978). Previous studies have inverted tomographic data sets of induced polarization measurements into subsurface models, using various approaches and parametrizations (e.g. Weller *et al.* 1996; Martin & Günther 2013; Johnson & Thomle 2018). Kemna (2000) introduced the first fully complex framework for the inversion of complex impedance measurements into subsurface images of conductivity magnitude and phase, which has been used in various applications (e.g. Kemna *et al.* 2004; Williams *et al.* 2009; Flores Orozco *et al.* 2011, 2012; Weigand & Kemna 2017; Maierhofer *et al.* 2022). The inversion is based on a weighted-least squares (WLSQ) framework, using the Hermitian norm, in which data and model are both explicitly treated as complex variables. However, the WLSQ framework is not able to ensure that the model found by means of optimization appropriately fits the real and imaginary part of the data in the context of their individual error estimates, which are often available from the data acquisition process. The reason for this is the inability of the WLSQ scheme to account for the error estimates of

the complex data's real and imaginary parts individually. Another disadvantage of the scheme can be that the model regularization cannot be independently adjusted for real and imaginary parts, which may be detrimental if subsurface conductivity and polarizability are known to exhibit different spatial characteristics. By individually accounting for the error estimates of the real and imaginary part of the complex data, as well as by controlling the prior assumptions applied to the real and imaginary part of the complex model independently, an adequate fit of the complex data can be reached in a complex inversion, using the probabilistic framework introduced in this work. For the application to CR imaging, we discuss explicitly how the probabilistic framework relates to the established WLSQ framework, as well as to the approach recently presented by Wang *et al.* (2023). Our implementation of the probabilistic framework for the inversion of CR measurements uses the forward modelling and inversion capabilities provided by the open-source software package pyGIMLi (Rücker *et al.* 2017).

The remainder of this follows: We introduce the probability distributions underlying the probabilistic framework and discuss simplifications, followed by a description of the Gauss–Newton approach that is used to solve the inverse problem by means of optimization. After that, we provide a short introduction into CR measurements and the established WLSQ inversion approach to invert them, which is used as a reference. Different aspects of the probabilistic framework are then demonstrated on synthetic examples. Finally, we discuss and conclude our results.

## 2 A PROBABILISTIC SOLUTION TO GEOPHYSICAL INVERSE PROBLEMS IN COMPLEX VARIABLES

The goal of geophysical inversion in complex variables is to recover a subsurface model  $\tilde{\mathbf{m}} \in \mathbb{C}^M$  from a set of data  $\tilde{\mathbf{d}} \in \mathbb{C}^N$ , given the forward operator  $\tilde{\mathbf{f}}(\tilde{\mathbf{m}})$ , as well as uncertainty estimates for the data and prior assumptions on spatial characteristics of the subsurface. The appropriate formulation of the underlying probability distributions in terms of complex random variables demands usage of the conjugate coordinate representation of complex vectors (e.g. Kreuz-Delgado 2009). For the complex vector  $\tilde{\mathbf{x}} \in \mathbb{C}^M$  we define  $\overset{c}{\mathbf{x}} \triangleq (\tilde{\mathbf{x}}, \tilde{\mathbf{x}}^*)^T \in \mathbb{C}^{2M}$  to be its representation in conjugate coordinates, with  $*$  denoting the complex conjugation and  $T$  denoting the transpose. The representation in conjugate coordinates is related to the representation of  $\tilde{\mathbf{x}}$  in terms of its real and imaginary part  $\overset{r}{\mathbf{x}} \triangleq (\mathbf{x}', \mathbf{x}'')^T \in \mathbb{R}^{2M}$  by the linear transformations

$$\overset{c}{\mathbf{x}} = \underbrace{\begin{bmatrix} \mathbf{I} & i\mathbf{I} \\ \mathbf{I} & -i\mathbf{I} \end{bmatrix}}_{\tilde{\mathbf{S}}} \overset{r}{\mathbf{x}} \quad (1)$$

and

$$\overset{r}{\mathbf{x}} = \tilde{\mathbf{S}}^{-1} \overset{c}{\mathbf{x}} = \frac{1}{2} \tilde{\mathbf{S}}^H \overset{c}{\mathbf{x}}, \quad (2)$$

with  $H$  denoting the conjugate transpose,  $\mathbf{I}$  denoting the identity matrix and  $i^2 = -1$ . The probabilistic inversion framework described in this work is built upon Bayes' theorem (Bayes 1763):

$$p(\overset{c}{\mathbf{m}} | \overset{c}{\mathbf{d}}) \propto p(\overset{c}{\mathbf{d}} | \overset{c}{\mathbf{m}}) p(\overset{c}{\mathbf{m}}). \quad (3)$$

The likelihood term  $p(\overset{c}{\mathbf{d}} | \overset{c}{\mathbf{m}})$  is combined with the prior term  $p(\overset{c}{\mathbf{m}})$  into the posterior distribution  $p(\overset{c}{\mathbf{m}} | \overset{c}{\mathbf{d}})$ , which assigns a conditional probability to a model realization  $\overset{c}{\mathbf{m}}$ , given the data  $\overset{c}{\mathbf{d}}$ . In order to

correctly describe data and model as complex random variables, eq. (3) features their representation in terms of conjugate coordinates.

Using the linear operator  $\tilde{\mathbf{S}}$ , it is theoretically possible to find an equivalent framework to the one described in this work using a real-valued parametrization of model and data, as described by Wang *et al.* (2023) for the inversion of CR measurements. However, formulating the inverse problem in terms of complex random variables is sensible if the mathematical description of the physical phenomenon underlying the measurements involves complex-valued parameters. Furthermore, in case of CR measurements, using a complex formulation illustrates how the probabilistic framework introduced in this work relates to the established complex inversion framework by Kemna (2000). We realize that a complex-valued model parametrization can have implications with regard to the use of generalized optimization packages. Although Wang *et al.* (2023) use a real-valued parametrization for the inversion, the forward calculation is nonetheless carried out using complex variables and the real and imaginary parts of the complex model response and complex sensitivity are extracted from the complex-valued results. While there might be benefits for specific applications, we do not see general advantages or disadvantages for either of the two approaches in terms of implementation.

### 2.1 Likelihood term

The model and data spaces are linked by the likelihood term. It describes the conditional probability of the data, given a certain model realization. If the errors of the complex data are assumed to be normal, we can formulate the likelihood as the following complex normal distribution (Picinbono 1996):

$$p(\overset{c}{\mathbf{d}} | \overset{c}{\mathbf{m}}) \propto \exp \left[ -\frac{1}{2} [(\tilde{\mathbf{d}} - \tilde{\mathbf{f}}(\tilde{\mathbf{m}}))^H, (\tilde{\mathbf{d}} - \tilde{\mathbf{f}}(\tilde{\mathbf{m}}))^T] \underbrace{\begin{pmatrix} \tilde{\Gamma}_d & \tilde{\mathbf{C}}_d \\ \tilde{\mathbf{C}}_d^H & \tilde{\Gamma}_d^* \end{pmatrix}^{-1}}_{=\overset{c}{\mathbf{R}}_d} \begin{pmatrix} \tilde{\mathbf{d}} - \tilde{\mathbf{f}}(\tilde{\mathbf{m}}) \\ (\tilde{\mathbf{d}} - \tilde{\mathbf{f}}(\tilde{\mathbf{m}}))^* \end{pmatrix} \right]. \quad (4)$$

Eq. (4) maps  $N$  complex data and their complex conjugates to a real-valued probability. The matrices  $\tilde{\Gamma}_d$  and  $\tilde{\mathbf{C}}_d$  capture the second-order properties of the complex normal distribution (eq. 4). Assuming error estimates for  $\mathbf{d}'$  and  $\mathbf{d}''$ , we find the complex covariance matrix (Picinbono 1996):

$$\begin{pmatrix} \tilde{\Gamma}_d & \tilde{\mathbf{C}}_d \\ \tilde{\mathbf{C}}_d^H & \tilde{\Gamma}_d^* \end{pmatrix} = 2 \tilde{\mathbf{S}} \begin{pmatrix} \text{Cov}(\mathbf{d}', \mathbf{d}') & \text{Cov}(\mathbf{d}', \mathbf{d}'') \\ \text{Cov}(\mathbf{d}'', \mathbf{d}') & \text{Cov}(\mathbf{d}'', \mathbf{d}'') \end{pmatrix} \tilde{\mathbf{S}}^{-1}. \quad (5)$$

Explicitly,  $\tilde{\Gamma}_d$  and  $\tilde{\mathbf{C}}_d$  can be calculated according to:

$$\tilde{\Gamma}_d = \text{Cov}(\mathbf{d}', \mathbf{d}') + \text{Cov}(\mathbf{d}'', \mathbf{d}'') + i(\text{Cov}(\mathbf{d}'', \mathbf{d}') - \text{Cov}(\mathbf{d}', \mathbf{d}')), \quad (6)$$

$$\tilde{\mathbf{C}}_d = \text{Cov}(\mathbf{d}', \mathbf{d}') - \text{Cov}(\mathbf{d}'', \mathbf{d}'') + i(\text{Cov}(\mathbf{d}'', \mathbf{d}') + \text{Cov}(\mathbf{d}', \mathbf{d}'')). \quad (7)$$

A first simplification can be derived if the error estimates of  $\mathbf{d}'$  and  $\mathbf{d}''$  are uncorrelated:

$$\text{Cov}(\mathbf{d}'', \mathbf{d}') = \text{Cov}(\mathbf{d}', \mathbf{d}'') = \mathbf{0}, \quad (8)$$

leading to  $\tilde{\Gamma}_d = \Gamma'_d$  and  $\tilde{\mathbf{C}}_d = \mathbf{C}'_d$ . Furthermore, if the error estimates of  $\mathbf{d}'$  and  $\mathbf{d}''$  are equal, we find:

$$\tilde{\mathbf{C}}_d = \text{Cov}(\mathbf{d}', \mathbf{d}') - \text{Cov}(\mathbf{d}'', \mathbf{d}'') = \mathbf{0}. \quad (9)$$

Given these two simplifications, eq. (4) reduces to

$$p(\tilde{\mathbf{d}}|\tilde{\mathbf{m}}) \propto \exp \left[ -(\tilde{\mathbf{d}} - \tilde{\mathbf{f}}(\tilde{\mathbf{m}}))^H \tilde{\Gamma}_d^{-1} (\tilde{\mathbf{d}} - \tilde{\mathbf{f}}(\tilde{\mathbf{m}})) \right]. \quad (10)$$

## 2.2 Prior term

We adapt the above concept to formulate the prior term, apply independent regularization to  $\mathbf{m}'$  and  $\mathbf{m}''$ , using the symmetric real operators  $\mathbf{R}_{\Re, \Im} = \lambda_{\Re, \Im} (\mathbf{W}_m^T \mathbf{W}_m)_{\Re, \Im}$ , with regularization strengths  $\lambda_{\Re}$  and  $\lambda_{\Im}$ , and find the following expression:

$$p(\tilde{\mathbf{m}}) \propto \exp \left[ -\frac{1}{2} [(\tilde{\mathbf{m}} - \tilde{\mathbf{m}}_p)^H, (\tilde{\mathbf{m}} - \tilde{\mathbf{m}}_p)^T] \underbrace{\begin{pmatrix} \mathbf{R}_{\Re} + \mathbf{R}_{\Im} & \mathbf{R}_{\Re} - \mathbf{R}_{\Im} \\ \mathbf{R}_{\Re} - \mathbf{R}_{\Im} & \mathbf{R}_{\Re} + \mathbf{R}_{\Im} \end{pmatrix}}_{=\tilde{\mathbf{R}}_m} \begin{pmatrix} \tilde{\mathbf{m}} - \tilde{\mathbf{m}}_p \\ (\tilde{\mathbf{m}} - \tilde{\mathbf{m}}_p)^* \end{pmatrix} \right], \quad (11)$$

with the prior model  $\tilde{\mathbf{m}}_p \in \mathbb{C}^M$ . Here, the inverse prior covariance matrix can be calculated according to

$$\tilde{\mathbf{R}}_m = 2 \tilde{\mathbf{S}} \begin{pmatrix} \mathbf{R}_{\Re} & \mathbf{0} \\ \mathbf{0} & \mathbf{R}_{\Im} \end{pmatrix} \tilde{\mathbf{S}}^{-1}. \quad (12)$$

The matrices  $\mathbf{R}_{\Re}$  and  $\mathbf{R}_{\Im}$  can exhibit different regularization characteristics. Setting  $\mathbf{R}_{\Re} = \mathbf{R}_{\Im} = \mathbf{R}$  leads to

$$p(\tilde{\mathbf{m}}) \propto \exp \left[ -(\tilde{\mathbf{m}} - \tilde{\mathbf{m}}_p)^H \mathbf{R} (\tilde{\mathbf{m}} - \tilde{\mathbf{m}}_p) \right], \quad (13)$$

applying equal regularization to  $\mathbf{m}'$  and  $\mathbf{m}''$ .

## 2.3 Optimization of the posterior distribution

We find the MAP model by maximizing eq. (3), which can be achieved by minimizing the corresponding cost function

$$\Psi(\tilde{\mathbf{m}}) = -\ln \left( p(\tilde{\mathbf{m}} | \tilde{\mathbf{d}}) \right). \quad (14)$$

Minimizing a cost function that maps a complex variable to a real-valued output is non-trivial, because such a cost function does not fulfil the Cauchy–Riemann equations and is therefore not complex differentiable. However, formulating the complex model vector in terms of conjugate coordinates allows us to exploit the differentiability of the cost function with respect to input from  $\mathbb{R}^{2M}$ . Due to the non-linear character of the forward operator  $\tilde{\mathbf{f}}(\tilde{\mathbf{m}})$ , eq. (14) has to be minimized iteratively. Sorber *et al.* (2012) formulate a generalized Gauss-Newton scheme for the solution of the minimization problem

$$\min_{\tilde{\mathbf{x}}} \|\tilde{\mathbf{F}}(\tilde{\mathbf{x}}, \tilde{\mathbf{x}}^*)\|^2. \quad (15)$$

Around a given model state  $\tilde{\mathbf{x}}_q$ , they approximate the non-linear function  $\tilde{\mathbf{F}}(\tilde{\mathbf{x}}, \tilde{\mathbf{x}}^*)$  using the first-order Taylor polynomial

$$\mathbf{t}_q^F(\Delta \tilde{\mathbf{x}}_q) = \tilde{\mathbf{F}}(\tilde{\mathbf{x}}_q) + \frac{\partial \tilde{\mathbf{F}}(\tilde{\mathbf{x}}_q)}{\partial \tilde{\mathbf{x}}^T} \Delta \tilde{\mathbf{x}}_q, \quad (16)$$

yielding the approximation  $\mathbf{t}_q^f$  of the objective function (eq. 15):

$$\mathbf{t}_q^f(\Delta \tilde{\mathbf{x}}_q) = \frac{1}{2} \left\| \mathbf{t}_q^F(\Delta \tilde{\mathbf{x}}_q) \right\|^2. \quad (17)$$

Here, the derivative operator with respect to the complex model in conjugate coordinates is given by

$$\frac{\partial}{\partial \tilde{\mathbf{x}}} = \left( \frac{\partial}{\partial \tilde{\mathbf{x}}}, \frac{\partial}{\partial \tilde{\mathbf{x}}^*} \right). \quad (18)$$

Explicitly, they find

$$\mathbf{t}_q^f(\Delta \tilde{\mathbf{x}}_q) = \frac{1}{2} \|\tilde{\mathbf{F}}_q\|^2 + \frac{1}{2} \Delta \tilde{\mathbf{x}}^T \begin{bmatrix} \tilde{\mathbf{J}}_q \mathbf{Q} \\ \tilde{\mathbf{J}}_q^* \mathbf{Q} \end{bmatrix}^H \begin{bmatrix} \tilde{\mathbf{F}}_q \\ \tilde{\mathbf{F}}_q^* \end{bmatrix} + \frac{1}{2} \Delta \tilde{\mathbf{x}}^H \tilde{\mathbf{J}}_q^H \tilde{\mathbf{J}}_q \Delta \tilde{\mathbf{x}}, \quad (19)$$

for the quadratic approximation of the objective function around  $\tilde{\mathbf{x}}_q$ ,

with  $\tilde{\mathbf{J}}_q = \frac{\partial \tilde{\mathbf{F}}(\tilde{\mathbf{x}}_q)}{\partial \tilde{\mathbf{x}}}$ ,  $\tilde{\mathbf{F}}_q = \tilde{\mathbf{F}}(\tilde{\mathbf{x}}_q)$  and

$$\mathbf{Q} = \begin{bmatrix} \mathbf{0} & \mathbf{I} \\ \mathbf{I} & \mathbf{0} \end{bmatrix}, \quad (20)$$

so that  $(\tilde{\mathbf{x}}, \tilde{\mathbf{x}}^*)^T = \mathbf{Q}(\tilde{\mathbf{x}}^*, \tilde{\mathbf{x}})^T$ . Setting the derivative with respect to  $\Delta \tilde{\mathbf{x}}^*$  equal to  $\mathbf{0}$  yields the condition for the minimum:

$$\frac{\partial \mathbf{t}_q^f(\Delta \tilde{\mathbf{x}}_q)}{\partial \Delta \tilde{\mathbf{x}}^*} = \frac{1}{2} \begin{bmatrix} \tilde{\mathbf{J}}_q \\ \tilde{\mathbf{J}}_q^* \mathbf{Q} \end{bmatrix}^H \begin{bmatrix} \tilde{\mathbf{F}}_q \\ \tilde{\mathbf{F}}_q^* \end{bmatrix} + \frac{1}{2} \begin{bmatrix} \tilde{\mathbf{J}}_q \\ \tilde{\mathbf{J}}_q^* \mathbf{Q} \end{bmatrix}^H \begin{bmatrix} \tilde{\mathbf{J}}_q \\ \tilde{\mathbf{J}}_q^* \mathbf{Q} \end{bmatrix} \Delta \tilde{\mathbf{x}}_q \stackrel{!}{=} \mathbf{0}. \quad (21)$$

In the condition for the minimum (eq. 21), we can identify the terms corresponding to the normal equations associated with the iterative minimization of eq. (14):

$$\tilde{\mathbf{B}}_q \Delta \tilde{\mathbf{m}}_q = \tilde{\mathbf{b}}_q, \quad (22)$$

$$\tilde{\mathbf{B}}_q = \left( \begin{bmatrix} \tilde{\mathbf{G}}_q & \tilde{\mathbf{G}}_q \\ \tilde{\mathbf{G}}_q^* & \tilde{\mathbf{G}}_q^* \end{bmatrix}^H \tilde{\mathbf{R}}_d \begin{bmatrix} \tilde{\mathbf{G}}_q & \tilde{\mathbf{G}}_q \\ \tilde{\mathbf{G}}_q^* & \tilde{\mathbf{G}}_q^* \end{bmatrix} + \tilde{\mathbf{R}}_m \right), \quad (23)$$

$$\tilde{\mathbf{b}}_q = \left( \begin{bmatrix} \tilde{\mathbf{G}}_q & \tilde{\mathbf{G}}_q \\ \tilde{\mathbf{G}}_q^* & \tilde{\mathbf{G}}_q^* \end{bmatrix}^H \tilde{\mathbf{R}}_d \begin{pmatrix} \tilde{\mathbf{d}} - \tilde{\mathbf{f}}(\tilde{\mathbf{m}}_q) \\ (\tilde{\mathbf{d}} - \tilde{\mathbf{f}}(\tilde{\mathbf{m}}_q))^* \end{pmatrix} - \tilde{\mathbf{R}}_m \begin{pmatrix} \tilde{\mathbf{m}}_q - \tilde{\mathbf{m}}_p \\ (\tilde{\mathbf{m}}_q - \tilde{\mathbf{m}}_p)^* \end{pmatrix} \right), \quad (24)$$

with

$$\tilde{G}_{ik} = \frac{\partial \tilde{f}_i}{\partial \tilde{m}_k}, \quad (25)$$

holding the partial derivatives of the forward operator with respect to the complex model, and

$$\tilde{\mathbf{E}}_{ik} = \frac{\partial \tilde{f}_i}{\partial \tilde{m}_k^*}, \quad (26)$$

holding the partial derivatives of the forward operator with respect to the complex conjugate of the complex model. If the forward operator is complex differentiable, as it is in case of the CR problem (Kemna 2000), the Cauchy–Riemann equations demand  $\tilde{\mathbf{E}} = \mathbf{0}$ . In that case, the imaginary part of  $\tilde{G}_{ik}$  holds the cross-sensitivities:

$$\frac{\partial f_i'}{\partial m_k''} = -\frac{\partial f_i''}{\partial m_k'}. \quad (27)$$

## 3 APPLICATION TO COMPLEX RESISTIVITY IMAGING

In CR imaging, forward modelling of the complex electric potential  $\tilde{\psi}$ , resulting for a given model realization and current source, is conducted by solving the Poisson equation at a given angular frequency  $\omega$ :

$$\nabla \cdot (\tilde{\sigma}(\omega) \nabla \tilde{\psi}(\omega)) - \nabla \cdot \tilde{\mathbf{j}}_s(\omega) = 0, \quad (28)$$

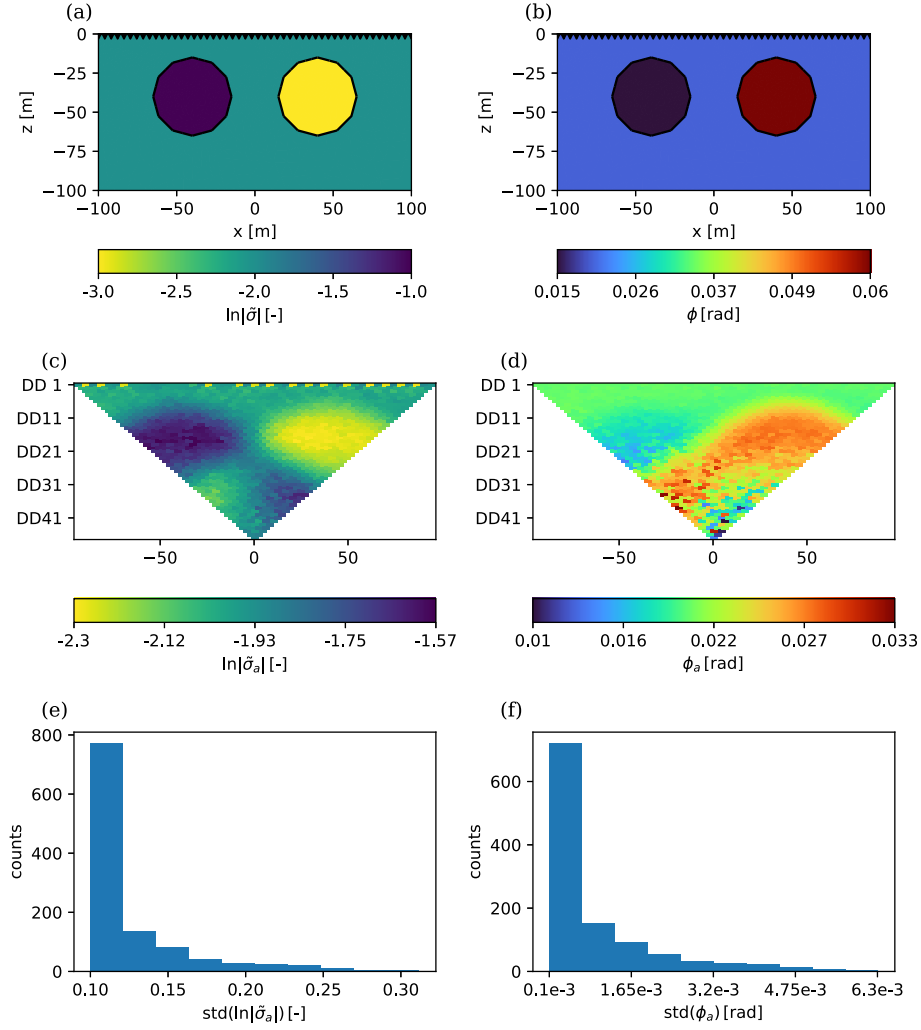


**Figure 1.** Conductivity magnitude (a) and phase (b) of the synthetic model and resultant impedance magnitude (c) and phase (d) pseudo-sections for a dipole–dipole measurement scheme (with pseudo-depth levels on vertical axis), subject to noise with the standard deviations shown in (e, f).

with the source current density  $\tilde{\mathbf{j}}_s$  and the complex electrical conductivity  $\tilde{\sigma}$ . This can be achieved, for example, by using the finite-difference method (e.g. Weller *et al.* 1996), or the finite-element method (e.g. Kemna 2000). The complex electrical impedance  $\tilde{z}$  is obtained as the ratio of the measured potential difference to the injected current. Kemna (2000) introduced the complex inversion of CR measurements into subsurface images of complex conductivity, explicitly treating data and model as complex variables. In this work, we adopt his transformation of the data and parametrization of the model. A set of  $N$  complex data

$$\tilde{d}_i = -\ln |\tilde{z}_i| + i\phi_i \quad (29)$$

with the complex electrical impedance  $\tilde{z}_i$  and negative phase of the complex electrical impedance  $\phi_i$ , is inverted into a subsurface model that features  $M$  parameters. The geometric factor  $k_i$  relates the complex electrical impedance to the apparent complex conductivity

$$\tilde{\sigma}_{a_i} = \frac{1}{k_i \tilde{z}_i}, \quad (30)$$

which we use for the visual display of CR data in pseudo-sections. The model is formulated as the complex logarithm of the complex

electrical conductivity:

$$\tilde{m}_k = \ln(\tilde{\sigma}_k) = \ln |\tilde{\sigma}_k| + i\phi_k, \quad (31)$$

with the phase of the complex electrical conductivity  $\phi_k$ . For reasons of readability, we refer to the real and imaginary parts of the complex data  $\tilde{d}_i$  as the *impedance magnitude* and *impedance phase*, since these are the parts of the measured complex electrical impedance  $\tilde{z}$  they represent. Consistently, we refer to the real and imaginary part of the complex model  $\tilde{m}_k$  as *conductivity magnitude* and *conductivity phase*, since they represent the magnitude and phase of the imaged complex electrical conductivity  $\tilde{\sigma}$ .

Kemna (2000) solves the CR inverse problem by minimizing the cost function

$$\Psi(\tilde{\mathbf{m}}) = (\tilde{\mathbf{d}} - \tilde{\mathbf{f}}(\tilde{\mathbf{m}}))^H \tilde{\mathbf{W}}_d^H \tilde{\mathbf{W}}_d (\tilde{\mathbf{d}} - \tilde{\mathbf{f}}(\tilde{\mathbf{m}})) + \lambda (\tilde{\mathbf{m}} - \tilde{\mathbf{m}}_p)^H \mathbf{W}_m^T \mathbf{W}_m (\tilde{\mathbf{m}} - \tilde{\mathbf{m}}_p), \quad (32)$$

with  $\tilde{\Gamma}_d^{-1} = \tilde{\mathbf{W}}_d^H \tilde{\mathbf{W}}_d$  and  $\mathbf{R} = \lambda \mathbf{W}_m^T \mathbf{W}_m$ . The data weighting matrix  $\tilde{\mathbf{W}}_d$  holds the inverses of the complex data errors

$$\tilde{\mathbf{e}}_i = \text{std}(\ln |\tilde{z}_i|) + i \text{std}(\phi_i) \quad (33)$$

as diagonal elements. Since equal weight is applied to the real and imaginary part of the complex residual  $(\tilde{\mathbf{d}} - \tilde{\mathbf{f}}(\tilde{\mathbf{m}}))$ , this WLSQ

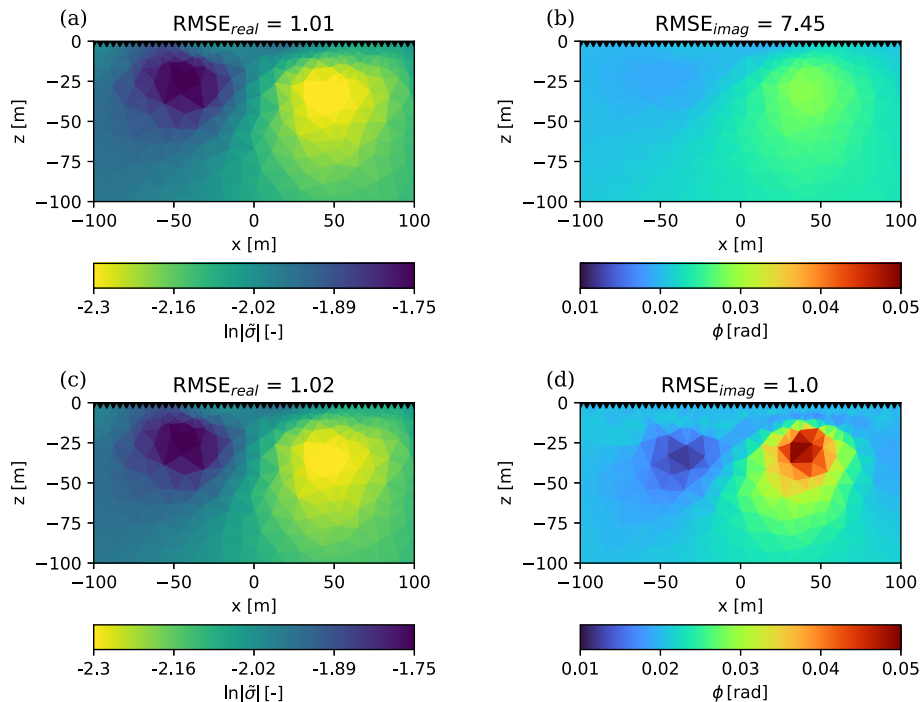


**Figure 2.** Conductivity magnitude (a, c) and phase (b, d) images resulting from the inversion of the synthetic data (compare Fig. 1) using the WLSQ framework (a, b) and the probabilistic framework (c, d).

framework implicitly assumes equal error estimates for impedance magnitude and phase. Furthermore, the same regularization strength is applied to the conductivity magnitude and phase. If we interpret eq. (32) from a probabilistic point of view, the data misfit term corresponds to the simplified likelihood term in eq. (10) and the regularization term corresponds to the simplified prior term in eq. (13). It is not guaranteed that a model minimizing eq. (32) achieves appropriate individual data fits for impedance magnitude and phase. Kemna (2000) overcomes this problem by refining the conductivity phase independently, after a solution for the conductivity magnitude has been found. During this final phase improvement, the conductivity magnitude is kept fixed and changes in the data fit of the impedance magnitude caused by cross-sensitivities are effectively disregarded, introducing inconsistencies with regard to the estimation of the MAP solution. Wang *et al.* (2023) provide a detailed comparison of the WLSQ inversion with final phase improvement to other complex resistivity inversion approaches. In the synthetic studies that follow, we use inversion results obtained from the minimization of eq. (32) as a reference, without a subsequent refinement of the conductivity phase, since we want to stay consistent during our comparison of the WLSQ framework and the probabilistic framework.

The two measured quantities  $\ln|\tilde{z}_i|$  and  $\phi_i$  are assumed to be subject to normally distributed noise. For the impedance magnitude, the typically used error model is linear in  $|\tilde{z}_i|$  (e.g. LaBrecque *et al.* 1996):

$$\text{std}(|\tilde{z}_i|) = a|\tilde{z}_i| + b. \quad (34)$$

The standard deviation of the impedance phase is assumed to be constant in some studies (e.g. Kemna 2000), or is assumed to follow an inverse power law (e.g. Flores Orozco *et al.* 2012)

$$\text{std}(\phi_i) = a|\tilde{z}_i|^{-b} + c, \quad (35)$$

extended by an absolute error  $c$ . There is no inherent condition that suggests for the error estimates of impedance magnitude and phase to be of similar size. To quantify how well a model response fits the complex data, we use two different formulations of the root-mean-square error (RMSE):

$$\text{RMSE}_{real} = \sqrt{\frac{1}{N} (\mathbf{d}' - \mathbf{f}(\tilde{\mathbf{m}}))^T \text{Cov}(\mathbf{d}', \mathbf{d}')^{-1} (\mathbf{d}' - \mathbf{f}(\tilde{\mathbf{m}}))}, \quad (36)$$

$$\text{RMSE}_{imag} = \sqrt{\frac{1}{N} (\mathbf{d}'' - \mathbf{f}(\tilde{\mathbf{m}}''))^T \text{Cov}(\mathbf{d}'', \mathbf{d}'')^{-1} (\mathbf{d}'' - \mathbf{f}(\tilde{\mathbf{m}}''))}, \quad (37)$$

to isolate the data fits with regard to the impedance magnitude and phase.

### 3.1 Example I: Independent impedance magnitude and phase error estimates

First, we investigate the probabilistic framework's ability to account for differences in the error estimates of impedance magnitude and phase. Fig. 1 shows the true model over which a dipole-dipole survey was simulated to generate synthetic data. Using the error models given in eqs (34) and (35), synthetic noise was generated and added to the data set. For the error model of the impedance magnitude (eq. 34) we used  $a = 0.1$  and  $b = 10^{-6} \Omega$ , while for the error model of the impedance phase (eq. 35) we used  $a = 10^{-7}$ ,  $b = 0.9$  and  $c = 10^{-4}$  rad. Fig. 1 shows the pseudo-sections of the impedance magnitude and phase, as well as the distributions of the standard deviations associated with the synthetic data. No correlations were assumed between the impedance magnitude and phase errors, as well as between errors of different data points. The impedance magnitude error estimates are significantly larger than the impedance phase error estimates. As this situation strongly violates the implicit assumption underlying eq. (32), we expect that an inversion using

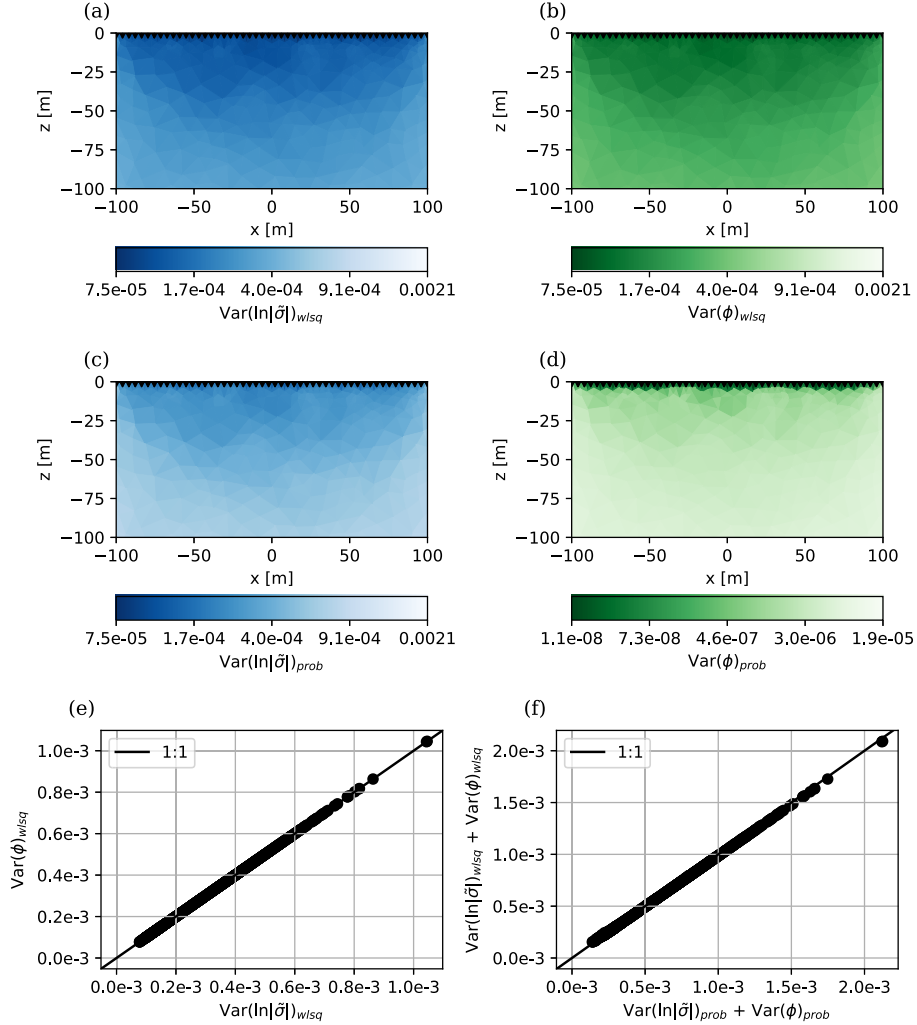


**Figure 3.** Estimated variances of the conductivity magnitude (a, c) and phase (b, d) according to eq. (40) for the WLSQ framework (a, b) and the probabilistic framework (c, d). Note the different colour scale in (d). Scatter of the conductivity phase variances against the conductivity magnitude variances, obtained for the WLSQ framework (e). Scatter of the added conductivity magnitude and phase variances for the WLSQ and probabilistic framework (f).

the WLSQ framework is not able to reach an adequate data fit for both impedance magnitude and phase. For demonstration purposes we here compare the results of two inversions. First, we inverted the synthetic data using the WLSQ framework. For this we set

$$\tilde{\Gamma}_{d_{ii}} = \text{std}(\ln(|\tilde{z}_i|))^2 + \text{std}(\phi_i)^2, \quad (38)$$

and

$$\tilde{\mathbf{C}}_d = \mathbf{0}, \quad (39)$$

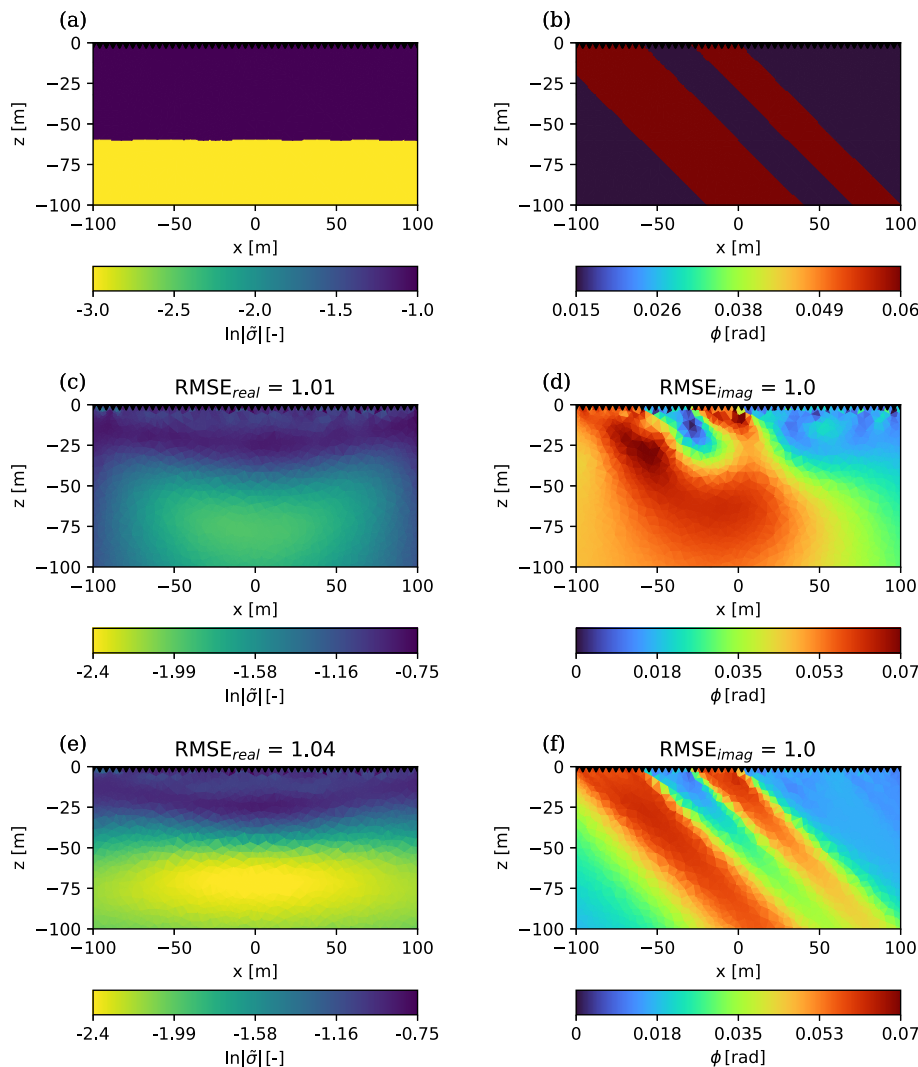
which implies equal error estimates for impedance magnitude and phase. The regularization strength  $\lambda$ , applied equally to the conductivity magnitude and phase, was fixed. Secondly, we inverted the synthetic data using the probabilistic framework. During this inversion, we included the error estimates of the impedance magnitude and phase appropriately in the complex data covariance matrix (eq. 5). For regularization, we fixed the individual values of  $\lambda_{\Re}$  and  $\lambda_{\Im}$  so that the obtained inversion result achieves a good data fit. Both inversions were performed on the same mesh using second-order smoothing between neighbouring cells, with a prior model  $\tilde{\mathbf{m}}_p = \mathbf{0}$ .

Fig. 2 shows the inversion results obtained from the WLSQ framework and the probabilistic framework, respectively. Both inversion

frameworks are able to fit the impedance magnitudes well, with  $\text{RMSE}_{\text{real}}$  values of 1.02 for the probabilistic framework and 1.01 for the WLSQ framework. Differences between the two inversion results occur for the data fit of the impedance phases. As indicated by the values of  $\text{RMSE}_{\text{imag}}$ , the probabilistic framework reaches the target data fit of 1.0, while the WLSQ framework underfits the impedance phases significantly, only reaching a  $\text{RMSE}_{\text{imag}}$  of 7.45. For the WLSQ framework, choosing a smaller value for  $\lambda$  would improve the data fit of the impedance phase. However, this would cause an overfitting of the impedance magnitude. Both approaches recover the synthetic model's magnitude equally well. For the conductivity phase, the probabilistic framework achieves a superior result.

For both inversion results, we approximated the posterior covariance matrix under the assumption of normally distributed model parameters near the MAP solution. We isolated the variances of the conductivity magnitude and phase according to (Picinbono 1996; Tarantola 2005)

$$\begin{pmatrix} \text{Cov}(\mathbf{m}', \mathbf{m}') & \text{Cov}(\mathbf{m}', \mathbf{m}'') \\ \text{Cov}(\mathbf{m}'', \mathbf{m}') & \text{Cov}(\mathbf{m}'', \mathbf{m}'') \end{pmatrix} = \frac{1}{2} \tilde{\mathbf{S}}^{-1} \begin{pmatrix} \mathbf{c}^H & \mathbf{c}^c & \mathbf{c}^c \\ \mathbf{G} & \mathbf{R}_d \mathbf{G} & \mathbf{R}_m \end{pmatrix}^{-1} \tilde{\mathbf{S}}. \quad (40)$$



**Figure 4.** Model used to create the synthetic data and recovered complex conductivity images. Conductivity magnitude (a) and phase (b) show strong macroscopic anisotropy. The conductivity magnitude and phase images displayed in (c) and (d) were recovered using isotropic geostatistical regularization. The conductivity magnitude and phase images displayed in (e) and (f) were recovered from an inversion, during which non-isotropic geostatistical regularization was applied independently to the conductivity magnitude and phase.

The estimated variances are displayed in Fig. 3. The conductivity magnitude and phase images obtained from the inversion with the probabilistic framework are subject to different variances, with the conductivity phase showing a significantly smaller uncertainty than the conductivity magnitude (compare Figs 3c and d). In contrast to this, the WLSQ framework implies equal error estimates for the impedance magnitude and phase in the likelihood term and equal regularization acting on the conductivity magnitude and phase in the prior term. This propagates into the posterior covariance matrix of the inversion result, causing equal variance estimates for the conductivity magnitude and phase (compare Figs 3a, b and e). The sum of the variances  $\text{Var}(\ln|\tilde{\sigma}|)$  and  $\text{Var}(\phi)$  is equal for both inversion frameworks (compare Fig. 3f). While  $\text{Var}(\phi)$  is smaller for the probabilistic framework, implying that interpretations on the basis of the conductivity phase obtained by the WLSQ framework might be too conservative,  $\text{Var}(\ln|\tilde{\sigma}|)$  is in fact larger for the probabilistic framework. This underestimation of the conductivity magnitude's uncertainty by the WLSQ framework might lead to false interpretations of the inversion result.

### 3.2 Example II: Independent conductivity magnitude and phase regularization

To demonstrate the probabilistic framework's ability to apply independent regularization to the conductivity magnitude and phase, we inverted data from a dipole–dipole survey that was simulated over the subsurface model shown in Figs 4(a) and (b). The synthetic model exhibits different structural characteristics in the magnitude and the phase of the subsurface conductivity. While the magnitude is horizontally layered, the layers of the phase show a dip of  $-45^\circ$ . During the inversion, we used non-isotropic geostatistical regularization operators provided by pyGIMLi (Rücker *et al.* 2017; Jordi *et al.* 2018), to account for the different dipping in conductivity magnitude and phase, and compared the results to the images obtained from an inversion with isotropic geostatistical regularization acting on the conductivity magnitude and phase. For both inversions, the regularization strengths were adjusted such that the data were appropriately fitted and the prior model was chosen to be  $\tilde{\mathbf{m}}_p = \mathbf{0}$ . The data error estimates of impedance magnitude and phase were accounted for accurately, according to eq. (5). The results obtained

from the two inversions (compare Fig. 4) demonstrate the advantage of using appropriate non-isotropic geostatistical regularization over isotropic regularization, in the present case. As the probabilistic framework introduced in this work is able to apply independent regularization on the conductivity magnitude and phase, setting it apart from the WLSQ framework, it is possible to account for the different structural characteristics and recover both parameter distributions well (compare Figs 4e and f). This is contrasted by the poor recovery of the parameters, especially of the conductivity phase, if the same structural characteristics are favoured by isotropic regularization acting on conductivity magnitude and phase (compare Figs 4c and d), as it is the case for the WLSQ framework [compare eqs (10) and (32)].

## 4 CONCLUSION

We introduced a probabilistic framework for the solution of geophysical inverse problems in complex variables. With regard to the inversion of CR measurements, the framework combines three key features whose importance has been demonstrated by Wang *et al.* (2023). First, it provides the possibility to account for independent error estimates of impedance magnitude and phase. This is essential to formulate the inverse problem in a consistent probabilistic sense, given that the error estimates of impedance magnitude and phase are not equal. While we demonstrated the application of the probabilistic framework for uncorrelated errors, correlations between errors of different data points, as well as between impedance magnitude and phase errors of the same data point, can be included according to eq. (5). Secondly, in order to impose independent regularization on the conductivity magnitude and phase, the respective model priors must be controlled individually. We achieve this by allowing for independent regularization operators to act on conductivity magnitude and phase. Thirdly, the probabilistic framework incorporates cross-sensitivities accurately via the imaginary part of  $\tilde{G}_{ik}$ , defined in eq. (25).

The probabilistic framework introduced in this work is built upon Bayes' theorem, combining a likelihood term and a model prior term into a posterior model distribution. The correct formulation of the underlying probability distributions, as well as the solution of the inverse problem by means of optimization, both demand usage of the conjugate coordinate representation of complex vectors. We solved the inverse problem resulting from the probabilistic formulation by means of Gauss–Newton optimization, estimating the MAP model under the posterior distribution. Between the probabilistic and WLSQ framework, the difference in computational cost comes down to the necessity to operate in a  $2N$ -dimensional complex data space and  $2M$ -dimensional complex model space in case of the probabilistic framework, while for the WLSQ framework this can be reduced to operation in a  $N$ -dimensional complex data space and  $M$ -dimensional complex model space. However, this is directly reflected in the inability of the WLSQ framework to account for independent error estimates on the real and imaginary part of the data, and to control the model priors acting on the real and imaginary part of the model individually. For the sake of simplicity, we estimated the variances of the recovered subsurface images under the assumption of normally distributed model-parameter uncertainties near the MAP model. We emphasize that value lies in the application of more advanced sampling approaches to the CR inverse problem, such as MCMC methods, which enable to perform an accurate error propagation and capture ambiguities associated with the solution of non-linear inverse problems. The probabilistic

framework for the solution of geophysical inverse problems in complex variables introduced in this work, provides a basis for such developments.

## ACKNOWLEDGMENTS

This work has been funded by the Deutsche Forschungsgemeinschaft (DFG, German Research Foundation) under Germany's Excellence Strategy, EXC-2070 - 390732324 - PhenoRob. This work was supported by the Open Access Publication Fund of the University of Bonn.

## DATA AVAILABILITY

All code used to generate the results shown in this paper is publicly available at <https://zenodo.org/doi/10.5281/zenodo.10280041>.

## REFERENCES

- Bayes, T., 1763. LII. An essay towards solving a problem in the doctrine of chances. By the late Rev. Mr. Bayes, F. R. S. communicated by Mr. Price, in a letter to John Canton, A. M. F. R. S., *Phil. Trans. R. Soc. Lond.*, **53**, 370–418.
- De Pasquale, G., Linde, N., Doetsch, J. & Holbrook, W.S., 2019. Probabilistic inference of subsurface heterogeneity and interface geometry using geophysical data, *Geophys. J. Int.*, **217**(2), 816–831, doi: 10.1093/gji/ggz055.
- Deng, S., Zhang, N., Kuang, B., Li, Y. & Sun, H., 2022. Bayesian markov chain monte carlo inversion of surface-based transient electromagnetic data, *SN Appl. Sci.*, **4**(10), 254, doi:10.1007/s42452-022-05134-5.
- Fichtner, A., Zunino, A. & Gebräud, L., 2019. Hamiltonian monte carlo solution of tomographic inverse problems, *Geophys. J. Int.*, **216**(2), 1344–1363, doi: 10.1093/gji/ggy496.
- Flores Orozco, A., Williams, K.H., Long, P.E., Hubbard, S.S. & Kemna, A., 2011. Using complex resistivity imaging to infer biogeochemical processes associated with bioremediation of an uranium-contaminated aquifer, *J. geophys. Res.*, **116**(G3), doi:10.1029/2010JG001591.
- Flores Orozco, A., Kemna, A. & Zimmermann, E., 2012. Data error quantification in spectral induced polarization imaging, *Geophysics*, **77**(3), E227–E237, doi: 10.1190/geo2010-0194.1.
- Johnson, T.C. & Thomle, J., 2018. 3-D decoupled inversion of complex conductivity data in the real number domain, *Geophys. J. Int.*, **212**(1), 284–296.
- Jordi, C., Doetsch, J., Günther, T., Schmelzbach, C. & Robertsson, J.O., 2018. Geostatistical regularization operators for geophysical inverse problems on irregular meshes, *Geophys. J. Int.*, **213**(2), 1374–1386, doi: 10.1093/gji/ggy055.
- Kemna, A., 2000. Tomographic inversion of complex resistivity: theory and application, *PhD thesis*, Ruhr Universität Bochum, Bochum, Germany.
- Kemna, A., Binley, A. & Slater, L., 2004. Crosshole ip imaging for engineering and environmental applications, *Geophysics*, **69**(1), 97–107, doi: 10.1190/1.1649379.
- Kreutz-Delgado, K., 2009. *The complex gradient operator and the CR-calculus*, arXiv doi:10.48550/arXiv.0906.4835.
- LaBrecque, D.J., Miletto, M., Daily, W., Ramirez, A. & Owen, E., 1996. The effects of noise on Occam's inversion of resistivity tomography data, *Geophysics*, **61**(2), 538–548, doi: 10.1190/1.1443980.
- Maierhofer, T., Hauck, C., Hilbich, C., Kemna, A. & Flores-Orozco, A., 2022. Spectral induced polarization imaging to investigate an ice-rich mountain permafrost site in Switzerland, *Cryosphere*, **16**(5), 1903–1925, doi: 10.5194/tc-16-1903-2022.
- Martin, T. & Günther, T., 2013. Complex resistivity tomography (CRT) for fungus detection on standing oak trees, *Eur. J. Forest Res.*, **132**, 765–776, doi: 10.1007/s10342-013-0711-4.

- Neal, R.M. *et al.*, 2011. Mcmc using hamiltonian dynamics, in *Handbook of Markov Chain Monte Carlo*, pp. 113–162, eds Brooks, S., Gelman, A., Jones, G.L. & Meng, X.-Li, Chapman & Hall/CRC, doi: 10.48550/arXiv.1206.1901.
- Pelton, W.H., Ward, S., Hallof, P., Sill, W. & Nelson, P.H., 1978. Mineral discrimination and removal of inductive coupling with multifrequency IP, *Geophysics*, **43**(3), 588–609, doi: 10.1190/1.1440839.
- Picinbono, B., 1996. Second-order complex random vectors and normal distributions, *IEEE Trans. Sig. Process.*, **44**(10), 2637–2640, doi: 10.1109/78.539051.
- Rücker, C., Günther, T. & Wagner, F.M., 2017. pyGIMLi: An open-source library for modelling and inversion in geophysics, *Comput. Geosci.*, **109**, 106–123, doi: 10.1016/j.cageo.2017.07.011.
- Sambridge, M. & Mosegaard, K., 2002. Monte Carlo methods in geophysical inverse problems, *Rev. Geophys.*, **40**(3), 3–1, doi: 10.1029/2000RG000089.
- Sen, M.K. & Stoffa, P.L., 1996. Bayesian inference, Gibbs' sampler and uncertainty estimation in geophysical inversion1, *Geophys. Prospect.*, **44**(2), 313–350, doi: 10.1111/j.1365-2478.1996.tb00152.x.
- Sorber, L., Barel, M.V. & Lathauwer, L.D., 2012. Unconstrained optimization of real functions in complex variables, *SIAM J. Opt.*, **22**(3), 879–898, doi: 10.1137/110832124.
- Tarantola, A., 2005. *Inverse Problem Theory and Methods for Model Parameter Estimation*, Vol. **89**, SIAM.
- Van Voorhis, G., Nelson, P. & Drake, T., 1973. Complex resistivity spectra of porphyry copper mineralization, *Geophysics*, **38**(1), 49–60, doi: 10.1190/1.1440333.
- Wang, H., Zimmermann, E., Weigand, M., Vereecken, H. & Huisman, J.A., 2023. Comparison of different inversion strategies for electrical impedance tomography (EIT) measurements, *Geophys. J. Int.*, **235**(3), 2888–2899, doi: 10.1093/gji/ggad398.
- Weigand, M. & Kemna, A., 2017. Multi-frequency electrical impedance tomography as a non-invasive tool to characterize and monitor crop root systems, *Biogeosciences*, **14**(4), 921–939, doi: 10.5194/bg-14-921-2017.
- Weller, A., Gruhne, M., Börner, F.D. & Seichter, M., 1996. *Monitoring hydraulic experiments by complex conductivity tomography*, in *Symposium on the Application of Geophysics to Engineering and Environmental Problems*, pp. 745–754, Environmental & Engineering Geophysical Society, doi: 10.4133/1.2922452.
- Williams, K.H. *et al.*, 2009. Geophysical monitoring of coupled microbial and geochemical processes during stimulated subsurface bioremediation, *Environ. Sci. Technol.*, **43**(17), 6717–6723, doi: 10.1021/es900855j.